Available online at www.sciencedirect.com
SCIENCE DIRECT®
International Journal of Solids and Structures 42 (2005) 1309–1326
INTERNATIONAL JOURNAL OF SOLIDS and STRUCTURES
www.elsevier.com/locate/ijsolstr

On the stability of penny-shaped cracks with friction: the five types of brittle behavior

Q.H. Zuo *, J.K. Dienes

Theoretical Division, Los Alamos National Laboratory, Los Alamos, NM 87545, USA

Received 30 July 2004; received in revised form 5 August 2004
Available online 18 September 2004

Abstract

The theory of penny-shaped cracks has been the subject of numerous investigations because of its conceptual simplicity and the feasibility of obtaining mathematical solutions. The simplicity of many of the final results makes the theory useful in many applications. This paper addresses a gap in the theory, the effect of interfacial friction in closed cracks and, in particular, its influence on the most unstable crack orientation and, hence, the compressive strength of materials. When friction is accounted for it is found that five types of brittle behavior are possible: **(a)** mode-I opening, **(b)** mixed opening and shear, **(c)** pure-shear without friction, and **(d)** shear with interfacial friction. A fifth type of behavior **(e)** which corresponds to a stable material response occurs when the compressive traction on the crack is so large that friction inhibits crack growth. The first four types, namely, **(a)**, **(b)**, **(c)**, **(d)** result in incipient material failure. The range of stress states for which each of the failure (incipient) types applies is given explicitly. Failure of a brittle material under triaxial test conditions is considered in detail to illustrate the results. An experiment performed by Howe et al. [Howe, P.M., Gibbons, G.G., Webber, P.E., 1985. An experimental investigation of the role of shearing initiation of detonation. In: Short, J.M. and Deal, W.E. (Eds.), Proceedings of the 8th International Symposium on Detonation, Albuquerque, NM] showing the response of a brittle material (TNT) to impact illustrates (perhaps surprisingly) behavior of types **(c)** and **(d)**. The chemical sensitivity of the TNT allows us to observe the effect of friction better than would be possible in a non-reactive material. The conditions that allow crack growth within the crack plane are discussed briefly.

Keywords: Penny-shaped cracks; Crack instability; Brittle materials; Brittle failure; Incipient failure

* Corresponding author. Tel.: +1 505 667 0377; fax +1 505 665 5926.
E-mail address: zuo@lanl.gov (Q.H. Zuo).

0020-7683/$ - see front matter © 2004 Elsevier Ltd. All rights reserved.
doi:10.1016/j.ijsolstr.2004.08.003

1. Introduction

The opening and strain energy of a penny-shaped crack in an infinite elastic medium were determined by Sack (1946) using oblate spheroidal coordinates, a solution appropriate when the deformation is axisymmetric. A related discussion by Sneddon (1946) approaches the same problem by means of dual integral equations and provides detailed information on the state of stress in the neighborhood of the crack tip. A subsequent paper by Segedin (1950) discusses the same geometry but the prescribed stress on the crack surface is uniform shear, and results are obtained by a method of "complex distances." The shear problem has also been addressed by Ulfyand (1963) using Mehler–Fok transforms. The general case, combining normal stress and shear, was addressed by Keer (1964, 1966). Different instability criteria were applied, depending on whether the crack is under tension (open crack) or under compression (closed crack). Fabrikant (1989) discusses many more complex aspects of the elastic theory of penny-shaped cracks, such as the deformation of elastic cracks in an anisotropic solid, under various kinds of loading, and the effect of variations in shape. He uses more elementary methods, arguing that such methods are more natural since the final results can be expressed with very simple algebraic expressions.

The physical situation is conceptually somewhat simpler for penny-shaped cracks than for two-dimensional cracks because the elastic response can be obtained by combining only two kinds of stress states (normal and shear), while for two-dimensional cracks Modes I, II, and III are distinguished. None of the papers cited above discusses the effect of interfacial friction. It is shown here that when friction is accounted for, an analysis of crack instability shows that there are five kinds of possible response rather than just the two discussed by Keer (1964, 1966).

The effect of interfacial friction in two-dimensional cracks has been addressed by a variety of authors who discuss its stabilizing influence. McClintock and Walsh (1962) study the effect of interfacial friction on the compressive strength of rocks. They assume that all crack orientations are equally likely and that failure occurs when the maximum local stress near the surface of the crack with the worst orientation reaches a critical value (the theoretical fracture strength of the material). They show that with a friction coefficient of unity the predicted compressive strength compares favorably with experimental data for a variety of rocks under different confining pressures. A good review of the roles of friction and failure statistics in brittle rapture is given by Alpa (1984), but the current paper differs from his and those referenced by him in focusing the analysis on penny-shaped cracks under a general, three-dimensional stress state.

The situation is complicated by the possible role of wing cracks, which may form and strongly affect the behavior of two-dimensional cracks under compression. Wing crack formation may occur in three-dimensional cracks as discussed by Kachanov (1982a,b), but it is not clear that the theory accounts for all possible modes of behavior. Guiton et al. (2003) assume a distribution of plane penny-shaped cracks and self-similar (homothetic) growth in their analysis of sedimentary layers. The formation of wing cracks is outside the scope of this paper, but it may be worth noting that under dynamical conditions shear cracks grow without the formation of wing cracks as discussed, for example, in recent work by Rosakis (2002) and references cited therein. The Rosakis paper discusses the formation of a planar melt layer in pseudotachylite that must have been formed by frictional heating. Wei and De Bremaecker (1994) provide an explanation for the dichotomy between static and dynamic behavior using energy considerations, as well as the reduced friction in preexisting cuts compared with that in newly formed crack surfaces. Rice (2000) discusses recent work by Heaton (1990) and others concerning the propagation of slip in geological faults, which are plane by implication, and refers to this behavior as self-healing rupture. In impact experiments on cut plates, Kalthoff and Winkler (1987) show that the cuts tend to extend more nearly in their own plane as impact speed increases, but the new surfaces may be considered to be shear bands rather that cracks in the classical sense. The relation of shear bands and shear cracks has not been fully clarified in the literature. The former presumes nonlinear thermo-plasticity and is typically treated as one dimensional, while the latter emphasizes brittle behavior in two or three dimensions and deals with linear elasticity. In real materials the situation is prob-

ably more complex than assumed in these idealizations, and may involve both kinds of behaviors where a brittle–ductile transition occurs. The impact experiments on artillery shells reported by Howe et al. (1985) show that cracks in TNT can propagate in their own plane, as discussed at the end of this paper. Of course, the most striking evidence of plane shear cracks is the formation of geological faults, but it may be argued that these involve preexisting damage.

In this paper, we extend McClintock and Walsh's work on interfacial friction in two-dimensional cracks to the failure analysis of brittle materials containing randomly oriented penny-shaped cracks. A general, three-dimensional loading, including the stress states where the principal stresses have mixed signs, is considered here, whereas McClintock and Walsh focus on triaxial compressive loading. It is also assumed here that all crack orientations are equally likely. Failure is assumed to initiate when the crack with the worst (critical) orientation becomes unstable. For a given stress state, we first find the critical orientation, then determine the load needed for the crack with that orientation to become unstable. Both open cracks and shear cracks with interfacial friction are studied. We use an extended Griffith energy-balance criterion which applies to both open cracks and closed cracks with friction (Dienes, 1983, 1984; Rice, 1984).

We find that for a general three-dimensional stress state, when friction is accounted for, five types of brittle behavior are possible: **(a)** mode-I opening, **(b)** mixed opening and shear, **(c)** pure-shear without friction, and **(d)** shear with interfacial friction. A fifth type of behavior **(e)** occurs when the compressive traction on the crack is so large that friction inhibits crack growth. The first four types, namely, **(a)**, **(b)**, **(c)**, **(d)** result in incipient material failure. The conditions for which each type of behavior applies are determined in terms of the stress biaxialities. For the stress states where incipient failure is possible, failure (critical crack) orientation is given analytically in the principal basis of the stress tensor.

The failure criteria are discussed in Section 2. The analysis of failure under a general, multi-axial state of stress is discussed in Section 3 and consists of three cases: Section 3.1, Open cracks, Section 3.2, Closed cracks and Section 3.3, Pure-shear cracks. The result of Section 3 is a list of candidate orientations for the critical crack. In Section 4, the candidates are compared to determine which is the most critical and the failure surface is obtained from failure analysis of the critical crack. This is done for all possible stress states. In Section 5, as an example, the important special case of triaxial tests (uniform lateral confinement) is discussed in detail. A summary and conclusions are given in Section 6.

The motivation for this analysis is to clarify the consequences of assuming an ensemble of penny-shaped cracks, the premise of a variety of modern damage theories obtained by synthesizing damage behavior with statistical concepts and specific defect theories (e.g., Dienes, 1996; Addessio and Johnson, 1990; Gambarotta and Lagomarsino, 1993). Thus, we do not examine possible variations from this premise but, rather, pursue this single premise in detail with a view to its application in formulating constitutive rules for the growth of damage.

2. Failure criteria

Consider the behavior of a brittle material containing a random, isotropic distribution of penny-shaped cracks with radius c subjected to a general three-dimensional loading. Neglecting the interactions between the cracks, incipient failure is assumed to occur when the crack with the critical orientation becomes unstable. The instability criterion for a penny-shaped crack, based on the Griffith energy-balance concept, including the effects of friction for closed cracks, is

$$F(\boldsymbol{\sigma}, \mathbf{n}, c) \equiv f(\boldsymbol{\sigma}, \mathbf{n}) - \frac{\pi}{2}\frac{2-\nu}{1-\nu}\frac{G\gamma}{c} = 0, \tag{1}$$

where $\boldsymbol{\sigma}$ is the remote stress tensor, assumed uniform, $\mathbf{n}$ is the unit normal to the crack, the elastic constants G and ν are the shear modulus and Poisson's ratio, and γ is the effective surface energy of the material. The

stress function $f(\boldsymbol{\sigma},\mathbf{n})$ depends on whether the crack is open (the normal component of traction is tensile) or closed (the normal component is compressive and controls the interfacial friction). For an open crack ($\sigma_n > 0$), both normal and shear stresses contribute to crack instability and the stress function $f(\boldsymbol{\sigma},\mathbf{n})$ is (Keer, 1964, 1966)

$$f(\boldsymbol{\sigma},\mathbf{n}) = f^{\mathrm{o}} = \left(1 - \frac{\nu}{2}\right)\sigma_n^2 + s_n^2, \tag{2}$$

where the normal and shear components of the remote traction are

$$\sigma_n \equiv \mathbf{n}\cdot\boldsymbol{\sigma}\mathbf{n}, \quad s_n \equiv \left[\mathbf{n}\cdot\boldsymbol{\sigma}^2\mathbf{n} - (\mathbf{n}\cdot\boldsymbol{\sigma}\mathbf{n})^2\right]^{1/2} \geqslant 0. \tag{3}$$

For the sake of compactness, the direct notation (e.g., Marsden and Hughes, 1983) for tensors and vectors is used throughout the paper. For a closed crack ($\sigma_n < 0$), the friction on the crack surface stabilizes the crack. If the Coulomb friction law is assumed to hold at the surface, then the stress function $f(\boldsymbol{\sigma},\mathbf{n})$ is (Dienes, 1983, 1984; Rice, 1984)

$$f(\boldsymbol{\sigma},\mathbf{n}) = f^{\mathrm{s}} = (s_n + \mu\sigma_n)^2 H(s_n + \mu\sigma_n), \tag{4}$$

where μ is the friction coefficient of the material and H is the Heaviside function, unity when the argument is positive and zero otherwise. A crack is in pure-shear when $\sigma_n = 0$, and Eqs. (2) and (4) both reduce to $f(\boldsymbol{\sigma},\mathbf{n}) = s_n^2$. It has been assumed in applying the instability condition for a penny-shaped crack (Eq. (1)) that the crack growth is homothetic (the crack grows in its own plane and its periphery remains circular). Though some criteria are known for growth that is not homothetic (e.g., Smith, 1971), they do not account for interfacial friction. The known differences from the homothetic case are small, on the order of 5% (Smith, 1971; Mura, 1991).

The crack instability surface $F(\boldsymbol{\sigma},\mathbf{n},c) = 0$ in the σ_n–τ_n plane is plotted in Fig. 1. It is interesting to note that the instability surface for a closed crack coincides with the Mohr–Coulomb failure envelope with the cohesion of the material taken as $\sqrt{\pi(2-\nu)G\gamma/2c(1-\nu)}$. The failure criterion based on the instability condition for a penny-shaped crack provides a justification for the Mohr–Coulomb criterion for brittle materials and the means to relate the cohesion constant to the defects (crack radius) in the materials. For an open crack, the instability surface is an ellipse with the major axis along σ_n, whereas the Mohr–Coulomb envelope extends to the tensile region with the same slope (the friction coefficient) as in the compressive

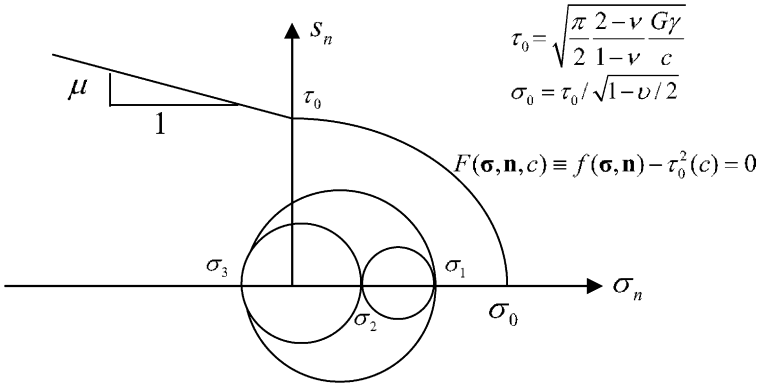

Fig. 1. The failure surface (defined by the onset of crack instability) for combined shear (s_n) and normal (σ_n) stresses on a penny-shaped crack with interfacial friction. Note that the result is similar to that for Mohr–Coulomb failure, but here the strength depends on crack dimensions. G denotes shear modulus; ν, Poisson's ratio; c, crack radius; and τ_0, shear strength. Mohr circles are also shown. The point at $\sigma_n = 0$ includes a range of frictionless shear cracks, discussed in Sections 3.3 and 4.3.

region. The ellipticity of the surface in the tensile region depends on Poisson's ratio and is close to zero. The brittle failure surface used here is an alternative to the Mohr–Coulomb criterion in the tensile stress regime.

For a fixed stress state, the function $f(\boldsymbol{\sigma}, \mathbf{n})$ depends on the crack orientation defined by the normal vector $\mathbf{n}$. As an example, consider a material subjected to a triaxial compression (uniform lateral confining pressure). The stress state is given by $\sigma_1 = -p$, $\sigma_2 = \sigma_3 = -rp$ where p is the loading parameter ($p > 0$) and r is the stress biaxiality. Let θ be the angle the crack normal $\mathbf{n}$ makes with the σ_1 loading direction. Since $f(\boldsymbol{\sigma}, \mathbf{n})$ is quadratic in the stresses it can be written as $f(\boldsymbol{\sigma}, \mathbf{n}) = p^2 g(\theta, r)$. For every stress state (fixed value of r), there is a critical load parameter $p^{\mathrm{cr}}(\theta, r)$ at which the crack with angle θ first becomes unstable. The critical loading is found from Eq. (1) as

$$p^{\mathrm{cr}}(\theta, r) = \frac{S_{\mathrm{cr}}(c)}{\sqrt{g(\theta, r)}}, \quad S_{\mathrm{cr}}(c) \equiv \sqrt{\frac{\pi}{2} \frac{2 - \nu}{1 - \nu} \frac{G\gamma}{c}}, \tag{5a,b}$$

For a given material and maximum crack size c, the critical loading p^{cr} in Eq. (5a) varies with the crack angle θ through the orientation function $g(\theta, r)$. Fig. 2 shows $g(\theta, r)$ as a function of θ for various values of the stress biaxiality r between -1 and 0 representing stress states between pure-shear and uniaxial compression. It may be observed that for a given stress state the responses of cracks with different orientations differ dramatically. The critical orientation at which the orientation function $g(\theta, r)$ reaches the maximum changes from 45° for $r = -1$ (pure-shear) to 64.8° for $r = 0$ (uniaxial compression). In Fig. 2, the Poisson's ratio and friction coefficient of the material are $\nu = 0.2$ and $\mu = 0.85$.

One can always search numerically through all crack orientations to find the critical crack orientation for a given stress state, but this requires search through two independent variables (such as the Euler angles), which can be computationally expensive. Furthermore, since the stress state in a material evolves during the loading process, one has to conduct the numerical search at every time step. As an alternative, we present the closed-form expression for the orientation of the critical crack for an arbitrary, three-dimensional stress state. The failure stresses are then found by applying Eq. (1) to the critical orientation.

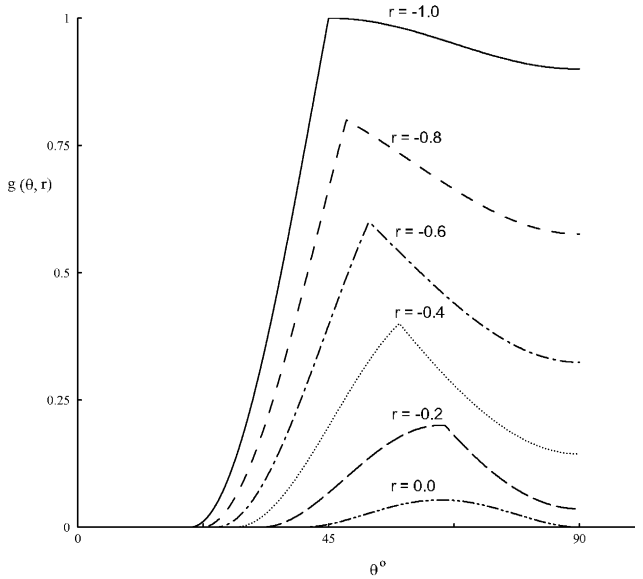

Fig. 2. Effects of crack orientation θ on the orientation functions $g(\theta, r)$, for several different stress states ranging from uniaxial compression to pure-shear. The critical orientation at which the orientation function $g(\theta, r)$ reaches the maximum changes from 45° for $r = -1$ (pure-shear) to 64.8° for $r = 0$ (uniaxial compression). The Poisson's ratio and friction coefficient are $\nu = 0.2$ and $\mu = 0.85$.

3. Failure analysis

For a given loading (i.e., $\boldsymbol{\sigma}$ is fixed), the critical (most unstable) crack orientation $\mathbf{n}^{\mathrm{cr}}$ is the one that maximizes the function $f(\boldsymbol{\sigma},\mathbf{n})$. Depending on the stress state, the crack with the critical orientation could be open without shear (mode I), open with shear, closed (with friction), or pure-shear (without friction).

The problem of finding the critical orientation $\mathbf{n}^{\mathrm{cr}}$ can be conveniently solved in the principal basis of the stress tensor $\boldsymbol{\sigma}$. Let $\boldsymbol{\sigma} = \sum_{i=1,3} \sigma_i \mathbf{e}_i \otimes \mathbf{e}_i$ where σ_1, σ_2, σ_3 and $\mathbf{e}_1$, $\mathbf{e}_2$, $\mathbf{e}_3$ are the principal stresses and principal stress directions, respectively, and the symbol $\otimes$ denotes the tensor product. The principal stresses are sorted in descending order (i.e., $\sigma_1 \geqslant \sigma_2 \geqslant \sigma_3$). A convenient way of relating σ_n and s_n to the principal stresses and the crack orientation is through the use of Mohr circles. The critical crack orientation corresponds to the point closest to the crack instability surface, as shown in Fig. 1. Since the Mohr circle for the σ_1–σ_3 plane encloses the other two Mohr circles, the closest point to the instability surface must be on this circle, that is, the critical crack normal lies in the σ_1–σ_3 (the maximum and minimum principal stress) plane.

Let θ denote the angle between $\mathbf{n}$ and the $\mathbf{e}_1$ axis ($0 \leqslant \theta \leqslant \pi/2$). Then the normal and shear components of the traction are

$$\begin{aligned} \sigma_n &= \frac{1}{2}((\sigma_1+\sigma_3)+(\sigma_1-\sigma_3)\cos 2\theta), \\ s_n &= \frac{1}{2}(\sigma_1-\sigma_3)\sin 2\theta \geqslant 0. \end{aligned} \tag{6a,b}$$

It follows immediately that $\sigma_3 \leqslant \sigma_n \leqslant \sigma_1$. Consequently, cracks can be open only when $\sigma_1 > 0$, closed when $\sigma_3 < 0$, and in pure-shear when $\sigma_1 > 0$ and $\sigma_3 < 0$.

The target function $\tilde{f}(\theta)$ to be maximized with respect to the crack orientation takes different forms depending on the sign of σ_n. For an open crack ($\sigma_n > 0$),

$$\tilde{f}^{\mathrm{o}}(\theta) = \frac{1}{4}\left\{\left(1-\frac{\nu}{2}\right)[\sigma_1+\sigma_3+(\sigma_1-\sigma_3)\cos 2\theta]^2 + (\sigma_1-\sigma_3)^2\sin^2 2\theta\right\}. \tag{7}$$

For a closed crack ($\sigma_n < 0$),

$$\tilde{f}^{\mathrm{c}}(\theta) = \frac{1}{4}\left\{((\sigma_1-\sigma_3)\sin 2\theta + \mu[\sigma_1+\sigma_3+(\sigma_1-\sigma_3)\cos 2\theta])^2\right\}. \tag{8}$$

The candidates for the critical crack orientation are solved by setting $\tilde{f}'(\theta) = 0$. Additionally, there is the pure-shear crack candidate whose orientation is found from the definition $\sigma_n(\theta^{\mathrm{s}}) = 0$. In the following three subsections, we present the expressions for the candidate orientations, according to the status of the critical crack (open, closed, pure-shear).

3.1. Open crack ($\sigma_n > 0$)

There are two candidate solutions to $\tilde{f}'(\theta) = 0$:

3.1.1. Pure-opening

This corresponds to mode-I opening with the crack normal along the maximum principal stress direction ($\theta^{\mathrm{o}} = 0$). Substitution of the solution into Eq. (2) gives the value of the stress function as $f^{\mathrm{o}} = (1-\nu/2)\sigma_1^2$. This open crack candidate exists when $\sigma_1 > 0$.

3.1.2. Open with shear

The orientation of the candidate crack is found to be

$$\theta^{\mathrm{os}} = \frac{1}{2}\cos^{-1}\left\{\left(\frac{2}{\nu}-1\right)\frac{1+r_{13}}{1-r_{13}}\right\}, \tag{9}$$

where $r_{13} \equiv \sigma_3/\sigma_1$ denotes the stress biaxiality. Since $-1 \leqslant \cos\theta^{os} \leqslant 1$, the mixed-candidate crack exists only for a limited range of stress states in which the material is in tension–compression ($\sigma_1 > 0, \sigma_3 < 0$),

$$-\frac{1}{(1-\nu)} \leqslant r_{13} \leqslant -(1-\nu) \tag{10}$$

It was assumed earlier that the crack is open ($\sigma_n > 0$); we now need to confirm that the candidate solution satisfies the assumptions. With the orientation given in Eq. (9), the normal component of the remote traction becomes

$$\sigma_n = \sigma_1(1 + r_{13})/\nu \tag{11}$$

Since $\sigma_1 > 0$, the candidate crack is open if $r_{13} > -1$, namely, σ_1 needs to be larger than the magnitude of σ_3. Combined with inequality (10), we find the complete range where this candidate solution is valid:

$$-1 < r_{13} \leqslant -(1-\nu). \tag{12}$$

The corresponding crack orientations at the limits are $\theta^{os} = 45°$ and $\theta^{os} = 0°$, respectively. In terms of the load angle $\beta \equiv \tan^{-1} r_{13}$, the range of stress states for a material with Poisson's ratio $\nu = 0.2$ corresponds to $-45° \leqslant \beta \leqslant -38.7°$. Substitution of the expression for the candidate orientation into Eq. (7) yields the value of the target function at the candidate orientation as

$$f^{os} = f(\sigma_1, r_{13}, \theta^{os}) = \left\{\left(\frac{2}{\nu} - 1\right)(1 + r_{13})^2 + (1 - r_{13})^2\right\}\frac{\sigma_1^2}{4}. \tag{13}$$

At the lower limit $r_{13} = -1$, the function takes the value $f(\sigma_1, -1, \theta^{os}) = \sigma_1^2$. At the upper limit $r_{13} = -(1-\nu)$, it follows from Eq. (13) that $f(\sigma_1, -(1-\nu), \theta^{os}) = (1 - \nu/2)\sigma_1^2$. Recall that $f^{o} = (1 - \nu/2)\sigma_1^2$ for the mode-I pure-opening candidate along $\mathbf{e}_1$ axis. Hence, at the upper limit $r_{13} = -(1-\nu)$ where the mixed-mode crack first becomes a candidate, the two candidates are equally critical, as expected since the mixed-mode crack degenerates to a mode-I crack here with $\theta^{o} = 0°$. Since $\partial f^{os}/\partial r_{13} = \sigma_1^2(1 + r_{13} - \nu)/\nu \leqslant 0$, we have $f^{os} \geqslant f^{o}$. Therefore, while a mode-I opening crack with the normal along the $\mathbf{e}_1$ axis is always a valid candidate, the mixed-mode candidate is more critical for $-1 < r_{13} \leqslant -(1-\nu)$, namely when the material is under nearly equal tension–compression loading.

In summary, there are at most two open crack candidates for the critical crack: a pure-opening crack, and a crack under a combination of opening and shear. The pure-opening candidate exists for all stress states with $\sigma_1 > 0$. The mixed candidate exists and dominates over a small region in the stress plane where the tension and compression are nearly equal in magnitude.

3.2. Closed (shear) cracks ($\sigma_n < 0$)

The solution of $f'(\theta) = 0$, with $f(\theta)$ given by Eq. (8), is

$$\theta^{c} = \frac{\pi}{4} - \frac{1}{2}\tan^{-1}\mu \tag{14}$$

The same expression was found by McClintock and Walsh (1962) for two-dimensional cracks by maximizing the local tensile stress around the crack surface. Recall that the failure criterion used here is an extended Griffith energy criterion (Eq. (1)), and the cracks are assumed to be penny-shaped (three-dimensional). As we have noted in Section 2, the instability surface for a closed crack coincides with the Mohr–Coulomb failure envelope; the critical closed crack found here coincides with the failure plane predicted by the Mohr–Coulomb failure criterion (see, for example, Lubliner, 1990).

It follows from Eq. (14) that $0 < \theta^c \leqslant 45\,^\circ$. When the material is subjected to a uniaxial compression, Eq. (14) predicts that the critical crack plane is tilted toward the loading axis $\mathbf{e}_3$. The predicted critical crack plane becomes more nearly parallel to the loading axis as the friction coefficient μ increases, consistent with the laboratory observed failure mode for brittle materials under uniaxial compression (Dienes, 1983; Schreyer and Wang, 1990).

Since we are considering closed cracks, the solution is valid only when the candidate crack is under compression and the applied shear overcomes the interfacial friction, i.e., $s_n > -\mu\sigma_n > 0$. When dealing with closed cracks, it is more convenient to treat the compressive principal stress (σ_3) as the primary, and to define $r_{31} \equiv \sigma_1/\sigma_3 = 1/r_{13}$. Since $\sigma_3 < 0$, with the substitution of the critical crack orientation given in Eq. (14) into Eq. (6a, b), the condition $\sigma_n < 0$ is found to require

$$r_{31} > -(\sqrt{\mu^2+1} - \mu)^2 \geqslant -1. \tag{15}$$

That is, if the maximum principal stress is tensile, the magnitude has to be somewhat less than the magnitude of the compressive principal stress.

Similarly, the requirement $s_n > -\mu\sigma_n$ yields

$$r_{31} < (\sqrt{\mu^2+1} - \mu)^2 \leqslant 1. \tag{16}$$

Thus, the two principal stresses have to differ enough to produce sufficient shear to overcome the friction on the crack surface. Combining inequalities (15) and (16) gives the range of stress states for which there exists a closed crack that is potentially unstable (it becomes unstable when the applied load is sufficiently large) as

$$-(\sqrt{\mu^2+1} - \mu)^2 < r_{31} < (\sqrt{\mu^2+1} - \mu)^2. \tag{17}$$

That is, a closed crack with interfacial shear is a valid candidate when the stress state falls into a sector centered about uniaxial compression along the $\mathbf{e}_3$ axis. The size of the sector decreases with the friction coefficient μ. For $\mu = 1.0$, the range is $-0.17 < r_{31} < 0.17$ ($-9.7^\circ < \beta_{31} < 9.7^\circ$, in terms of the load angle, $\beta_{31} \equiv \tan^{-1}\sigma_1/\sigma_3$). By substituting the expression for the critical crack orientation given by Eq. (14) into Eq. (8), the corresponding target function is found to be

$$f^c \equiv f(\sigma_3, r_{31}, \theta^c) = \frac{\sigma_3^2}{4}\{(\sqrt{\mu^2+1} - \mu) - (\sqrt{\mu^2+1} + \mu)r_{31}\}^2. \tag{18}$$

3.2.1. Friction-locked zone

When both principal stresses are compressive, all cracks are closed and there exists a range of stress states over which the cracks are always stable (locked) due to frictional resistance on the crack surface. The friction-locked zone, in terms of the range of stress biaxiality, is determined by the requirement $s_n \leqslant -\mu\sigma_n$, and may be inferred from Eq. (16) to be

$$(\sqrt{\mu^2+1} - \mu)^2 \equiv r_L \leqslant r_{31} \leqslant 1. \tag{19}$$

The size of the friction-locked zone can be better represented by the load angle (β_{31} is measured from the uniaxial compression axis along the direction of σ_3). Let $\bar{\beta} \equiv \tan^{-1}(\sqrt{\mu^2+1} + \mu)^2 - \pi/4$. Then it follows from Eq. (19) that $r_L = \tan(\pi/4 - \bar{\beta})$, so the wedge of size $\bar{\beta}$ starting from the bisector $\sigma_1 = \sigma_3 < 0$ represents the friction-locked zone in stress space. For $\mu = 1.0$, the lock angle is $\bar{\beta} = 35.3^\circ$. Fig. 3 shows the lock angle $\bar{\beta}$ as a function of the friction coefficient μ. The angle $\bar{\beta}$ starts at $0\,^\circ$ when the material is frictionless (hence any deviation from the hydrostatic compression can render some crack unstable when the load parameter is sufficiently large) and asymptotically approaches the limit of 45°; that is, if the friction coefficient is large enough nearly all cracks are stable when both principal stresses are compressive.

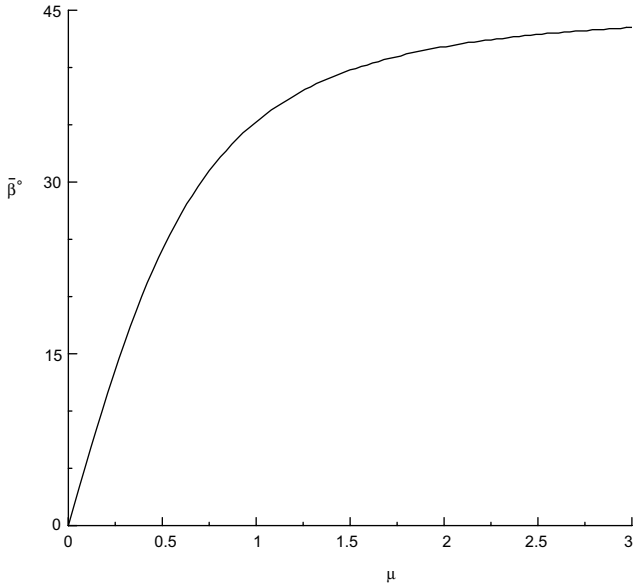

Fig. 3. Effects of friction coefficient, μ on the size of the friction-locked zone, $\bar{\beta}$. When the stress state falls inside a sector centered about hydrostatic compression state with size $2\bar{\beta}$, all cracks are stable because the interfacial friction exceeds the applied shear. The lock-angle $\bar{\beta}$ starts at 0° for $\mu = 0$, and asymptotically approaches the limit 45° for large values of μ.

3.3. Pure-shear cracks ($\sigma_n = 0$)

Since $\sigma_3 \leqslant \sigma_n \leqslant \sigma_1$, a non-trivial solution exists if and only if the principal stresses have mixed signs, $\sigma_1 > 0$, $\sigma_3 < 0$. The solution of the constraint equation $\sigma_n(\theta^s) = 0$ is

$$\theta^s = \tan^{-1}(1/\sqrt{-r_{13}}). \tag{20}$$

In general, this orientation does not correspond to the maximum shear plane, which is always at 45° from the principal stress axes. For the special situation when the material is under pure-shear, $\sigma_3 = -\sigma_1 < 0$, Eq. (20) gives $\theta^s = 45°$. The shear component on the crack surface is $s_n = 1/2(\sigma_1 - \sigma_3)\sin 2\theta^s = \sqrt{-r_{13}\sigma_1}$, and the corresponding value of the target function is

$$f^s \equiv s_n^2 = -r_{13}\sigma_1^2 = -\sigma_1\sigma_3 > 0 \tag{21}$$

This pure-shear candidate crack exists for all tension–compression stress states ($\sigma_1 > 0,\ \sigma_3 < 0$).

In summary, depending on the stress state, the candidates for the critical crack may be **(a)** pure-opening (mode-I), **(b)** mixed opening and shear, **(c)** pure-shear, and **(d)** shear with interfacial friction. Next, we will compare the values of the target functions corresponding to the candidate orientations to determine which is the critical crack. This will be done for all possible stress states.

4. Critical crack orientation and failure surface

Depending on the stress state, there can be several candidates for the critical crack with different orientations; the one with the largest value of the target function is the critical one. The failure stress is then determined by substituting $f(\boldsymbol{\sigma}, \mathbf{n}^{cr})$ into Eq. (1). In what follows we will divide the stress states into various regions and give the corresponding failure surfaces.

4.1. $\sigma_1 \geqslant \sigma_2 \geqslant \sigma_3 \geqslant 0$

The material is under pure tension, so the only candidates are the mode-I cracks with normal along the principal stress directions. Hence the critical crack normal is $\mathbf{n}^{\mathrm{cr}} = \mathbf{e}_1$, associated with $f^{\mathrm{cr}}(\boldsymbol{\sigma}, \mathbf{e}_1) = (1 - \nu/2)\sigma_1^2$. Substitution of the expression for f into Eq. (1) gives the tensile failure surface

$$F^{\mathrm{o}}(\boldsymbol{\sigma}, c) \equiv \sigma_1 - \frac{S_{\mathrm{cr}}}{\sqrt{1 - \nu/2}} = 0 \tag{22}$$

with $S_{\mathrm{cr}}(c)$ defined in Eq. 5a, b(5b). Hence, when under pure tension a brittle material fails when the maximum principal (tensile) stress reaches a critical value, which is the Rankine tensile failure criterion.

4.2. $\sigma_3 \leqslant \sigma_2 \leqslant \sigma_1 \leqslant 0$

The material is under pure compression and the cracks are either friction-locked (hence stable) when the principal stresses are sufficiently close (i.e., $(\sqrt{\mu^2 + 1} - \mu)^2 \leqslant r_{31} \leqslant 1$), or potentially unstable when the difference between shear and interfacial friction on some crack becomes large enough. For $r_{31} < (\sqrt{\mu^2 + 1} - \mu)^2$, there is one candidate closed crack with the orientation given by Eq. (14). The failure surface is found by substituting the expression for the target function in Eq. (18) into Eq. (1), and can be written, in terms of the principal stresses, as

$$F^{\mathrm{c}}(\boldsymbol{\sigma}, c, \mu) \equiv \sigma_3 - (\sqrt{\mu^2 + 1} + \mu)^2\sigma_1 + 2(\sqrt{\mu^2 + 1} + \mu)S_{\mathrm{cr}} = 0. \tag{23}$$

The surface coincides with the Mohr–Coulomb surface. The size of the failure surface (distance from the surface to the origin) increases with the friction coefficient and decreases with the radius of the largest crack in the material. In the σ_1–σ_3 plane the slope of the failure surface increases with the friction coefficient. The compressive strength of the material is found by setting $\sigma_1 = 0$ in Eq. (23)

$$\sigma_{\mathrm{c}} = |\sigma_3| = 2(\sqrt{\mu^2 + 1} + \mu)S_{\mathrm{cr}}. \tag{24}$$

It follows from substituting Eq. (22) and Eq. (24) that the ratio of the compressive strength to the tensile strength is

$$\frac{\sigma_{\mathrm{c}}}{\sigma_{\mathrm{t}}} = \sqrt{2(2 - \nu)}(\sqrt{\mu^2 + 1} + \mu). \tag{25}$$

Dienes (1983) found the critical crack orientation and the strength under uniaxial compression. Eq. (25) reproduces those results. However, here, Eq. (23) applies to a general state of stress, not just uniaxial compression. It is interesting to note that the critical crack orientation depends on the friction coefficient of the material, but not on the stress biaxiality (provided it is within the range given by Eq. (17)). The critical stress, on the other hand, increases with both the friction coefficient and the stress biaxiality.

4.3. $\sigma_1 > 0, \sigma_3 < 0$

Material is under tension–compression. This is the most interesting situation; there are at least two candidates (pure-opening and pure-shear) in this region of the stress state, and in certain sub-regions there is another candidate, either the mixed open and shear or shear with friction. We divide the solutions into two major groups, according to the relative magnitudes of the principal stresses.

4.3.1. $\sigma_1 \geqslant -\sigma_3 > 0$ $(-1 < r_{13} \leqslant 0)$

Since the principal stresses are of mixed signs, there are always two candidates, a pure-opening candidate crack with normal parallel to the $\mathbf{e}_1$ axis with $f^{\mathrm{o}} = (1 - \nu/2)\sigma_1^2$, and a pure-shear candidate crack with orientation given by Eq. (20) and $f^{\mathrm{s}} = -r_{13}\sigma_1^2 = -\sigma_1\sigma_3$.

4.3.1.1. $-(1-\nu) \leqslant r_{13} \leqslant 0$. The pure-opening and pure-shear cracks are the only candidates, and the critical one is the pure-opening crack with the failure surface given by Eq. (22). That is, the mode-I opening failure mode extends well into the tension–compression region.

4.3.1.2. $-1 \leqslant r_{13} \leqslant -(1-\nu)$. In this region, there is also a mixed opening and shear candidate. It is straightforward to verify that among the three candidates the mixed one is the most critical, with the orientation given by Eq. (9) and failure surface given by

$$F^{\mathrm{os}}(\boldsymbol{\sigma}, c) \equiv \left\{ \left(\frac{2}{\nu} - 1 \right) (\sigma_1 + \sigma_3)^2 + (\sigma_1 - \sigma_3)^2 \right\} - 4S_{\mathrm{cr}}^2 = 0 \tag{26}$$

The failure surface has an elliptical cross-section in the principal stress space.

4.4. $0 \leqslant \sigma_1 \leqslant -\sigma_3$ $(-\infty < r_{13} \leqslant -1)$

Material is under tension and compression, with compression dominating. In this region, there are again at least two candidates; pure-opening crack with the normal in the direction of the $\mathbf{e}_1$ axis and $f^{\mathrm{o}} = (1-\nu/2)\sigma_1^2$, and pure-shear crack with $f^{\mathrm{s}} = -r_{13}\sigma_1^2 = -\sigma_1\sigma_3$. Since $r_{13} \leqslant -1$, it follows immediately that $f^{\mathrm{s}} \geqslant \sigma_1^2 > f^{\mathrm{o}}$, i.e., the pure-shear candidate is always more critical than the pure-opening candidate. This region is further split into two sub-regions:

4.4.1. $-\left(\sqrt{\mu^2+1}+\mu\right)^2 \leqslant r_{13} \leqslant -1$

Here, the only candidates are the two discussed above and the pure-shear candidate is the more critical. The failure surface is given by

$$F^{\mathrm{ps}}(\sigma, c) = -\sigma_1\sigma_3 - S_{\mathrm{cr}}^2 = 0. \tag{27}$$

The failure surface has a hyperbolic cross-section in the principal stress space.

4.4.2. $-\infty \leqslant r_{13} \leqslant -\left(\sqrt{\mu^2+1}+\mu\right)^2$

Since the stress state is close to uniaxial compression, it is more convenient to work with $r_{31} = 1/r_{13}$ (see Section 3.2.). In this region, in addition to the two candidates discussed above, there is also a frictional-shear candidate, with the target function $f^{\mathrm{c}} = \sigma_3^2/4(\sqrt{\mu^2+1}-\mu-(\sqrt{\mu^2+1}+\mu)r_{31})^2$. At the lower limit $r_{31} = -(\sqrt{\mu^2+1}-\mu)^2$, $f^{\mathrm{s}} = -\sigma_1\sigma_3 = -r_{31}\sigma_3^2 = \sigma_3^2(\sqrt{\mu^2+1}-\mu)^2 = f^{\mathrm{c}}$, so the two candidates are equally critical. At the upper limit $r_{31} = 0$, we have $f^{\mathrm{s}} = 0$ and $f^{\mathrm{c}} = \sigma_3^2/4(\sqrt{\mu^2+1}-\mu)^2 > f^{\mathrm{s}}$. It can be readily shown that in this region of stress states the frictional-shear candidate is more or equally critical than the pure-shear candidate ($f^{\mathrm{c}} \geqslant f^{\mathrm{s}}$). The failure surface is given by Eq. (23).

In summary, the critical crack can be one of four types, namely, pure-opening, mixed opening and shear, pure-shear, or frictional shear, depending on the stress biaxiality. The corresponding failure (incipient) surface is given by one of Eqs. (22), (23), (26), and (27).

Similar failure surfaces were presented by Alpa (1984) for plane stress loadings. His results were based on the geometrical considerations of the limit domains in the Mohr plane. The detailed stability analysis of penny-shaped cracks under a general, three-dimensional stress state presented here elucidates our understanding of the various types of brittle behavior. Furthermore, while no explicit mention of the critical crack orientations was given in Alpa's work (though it can be inferred in some cases), we have presented explicit expressions for the critical crack orientation under all possible stress states. These expressions are useful in formulating a computer algorithm that accounts in detail for the accumulation of damage (Dienes et al., 2003).

An example of material behavior under triaxial loading is discussed in the next section to illustrate the results presented above.

5. Triaxial (tension/compression) test

As an example, let us now consider the failure of a brittle material under triaxial stress loading (the radial stresses are held equal during the test, $\sigma_{22} = \sigma_{33}$). Let $\sigma_{11} = p\ \cos\beta$ and $\sigma_{33} = p\sin\beta$ denote the axial and lateral stresses, respectively, where $p > 0$ is the loading parameter and the load angle β defines the state of stress in the material ($-\pi \leqslant \beta \leqslant \pi$). Since the shear components vanish we have $\sigma_1 = \sigma_{11}$, $\sigma_2 = \sigma_3 = \sigma_{33}$ for $-3\pi/4 \leqslant \beta \leqslant \pi/4$, and $\sigma_1 = \sigma_2 = \sigma_{22}$, $\sigma_3 = \sigma_{11}$ for $\pi/4 \leqslant \beta \leqslant \pi$ or $-\pi \leqslant \beta \leqslant -3\pi/4$. It is noted that $\beta = \pi$ and $\beta = -\pi$ both represent uniaxial compression along the axial (σ_{11}) direction, and the descending ordering of the principal stresses $\sigma_1 \geqslant \sigma_2 \geqslant \sigma_3$ is maintained. Due to the symmetry of loading, all cracks having the same angle with the axial loading (σ_{11}) axis respond equally to the applied stress. Hence, the failure orientation (the normal to the critical crack) can only be determined within a cone centered along the σ_{11} axis. Let θ be the angle the normal to the critical crack makes with the σ_{11} axis. We will study the effects of stress state on the failure angle θ. To study all possible stress states, one needs to probe through the range of load angle, $-\pi \leqslant \beta \leqslant \pi$. However, due to symmetry of the problem, we can limit our discussions to $-3\pi/4 \leqslant \beta \leqslant \pi/4$ ($\sigma_1 = \sigma_{11} \geqslant \sigma_3 = \sigma_{33}$). Then $\beta = 0$ corresponds to uniaxial tension in the axial direction and $\beta = -\pi/2$ corresponds to compression in the radial direction. Failure criteria for the remaining stress states can be inferred from those results.

5.1. $-3\pi/4 \leqslant \beta \leqslant -\pi/4$

In this region, the magnitude of the compressive stress is larger than the tensile stress ($-\sigma_3 \geqslant \sigma_1$) and the critical crack type is either pure-shear or shear with interfacial friction. This region can be further divided into three sub-regions. (1) $-3\pi/4 \leqslant \beta < -3\pi/4 + \bar{\beta}$ where $\bar{\beta}$ is the size of the friction-locked zone defined earlier. Here, all cracks are stable due to interfacial friction, and consequently, no failure surface exists in this region. (2) $-\pi/2 - \beta^{s} \leqslant \beta \leqslant -\pi/2 + \beta^{s}$ with $\beta^{s} \equiv \tan^{-1}(\sqrt{\mu^2 + 1} - \mu)^2 = \pi/4 - \bar{\beta}$. In this region, shear in the material is large enough to overcome the frictional resistance and the critical crack is a frictional shear crack. It follows from the definitions that $-3\pi/4 + \bar{\beta} = -\pi/2 - \beta^{s}$ so there is no gap between the friction-locked zone and the frictional shear failure region. The failure angle is given by Eq. (14), and the corresponding failure surface is given by Eq. (23). (3) $-\pi/2 + \beta^{s} \leqslant \beta \leqslant -\pi/4$. The critical crack is a pure-shear crack, with the failure angle θ given by Eq. (20) and the failure surface given by Eq. (27).

5.2. $-\pi/4 \leqslant \beta \leqslant \pi/4$

Here, the tensile principal stress is larger than the magnitude of the compressive principal stress ($\sigma_1 \geqslant -\sigma_3$) and the critical crack type is either pure-opening or mixed opening and shear. This region can further divided into two sub-regions: (1) $-\pi/4 \leqslant \beta \leqslant -\beta^{o}$, where $\beta^{o} \equiv \tan^{-1}(1 - \nu)$. The critical crack type is mixed opening and shear. The failure angle θ is given by Eq. (9), with the corresponding failure surface given by Eq. (26). (2) $-\beta^{o} \leqslant \beta \leqslant \pi/4$. The critical crack type is pure-opening with the normal in the axial loading (σ_{11}) direction ($\theta = 0^0$) and tensile-failure surface given by Eq. (22). At $\beta = \pi/4$, $\sigma_3 = \sigma_1$, the state of stress is hydrostatic and there is no unique critical orientation.

Fig. 4 plots the failure angle θ as a function of load angle β over the complete range of β ($-\pi \leqslant \beta \leqslant \pi$) for several values of the coefficient of friction between 0 and 2.0. The figure starts from the left with a uniaxial compression in the σ_{11} direction ($\beta/\pi = -1$) and since σ_{11} is the minimum stress $\sigma_3 = \sigma_{11}$, the failure angle with the loading direction is $90° - \theta_c$ with θ_c given by Eq. (14), in agreement with a previous result (Dienes, 1983). It may be observed that friction has a significant effect on failure orientation. For a frictionless material, the critical crack plane is the maximum-shear plane, which corresponds to $\theta = 45°$. As μ increases, the failure angle increases so that the failure plane becomes increasingly parallel to the loading axis. At $\mu = 2.0$, the failure plane is at 75° to the axial loading direction. In laboratory tests, it is often observed

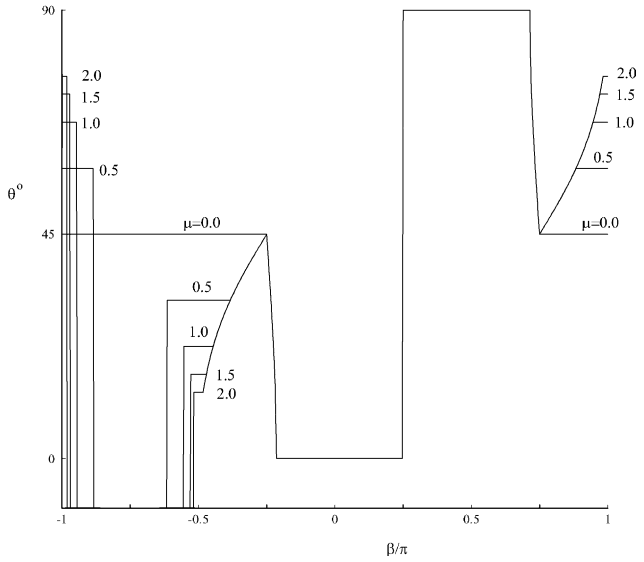

Fig. 4. Failure angle as a function of load angle for triaxial loading for several values of friction coefficient, μ. The nine regions are described in the text (the regions just above $\beta = -\pi$ and just below $\beta = \pi$ are considered as one region which represents nearly uniaxial compression). Proceeding from the left the types of failure are: axial splitting (shear with friction), friction-locked, radial splitting, pure-shear, mixed opening and shear, axial tensile failure, radial tensile failure, opening with shear, and pure-shear.

that brittle materials such as rocks and concretes display cracks almost parallel to the loading direction when subjected to a uniaxial compression (Dienes, 1983). This has also been observed in a brittle explosive (TNT) subjected to plate impact (Howe et al., 1985) as shown in Fig. 7.

As the load angle β increases from $-\pi$, the stress state changes from uniaxial compression to triaxial compression with increasing lateral confining stress. Fig. 4 shows that for a certain range of lateral confining pressure the failure type (shear with friction) and orientation remain the same as for uniaxial compression. The range depends on the coefficient of friction. Further increase in the confining stress stabilizes all cracks, as the material enters the friction-locked zone. For $-\pi \leqslant \beta \leqslant -\pi/2$, the curves are symmetrical about the hydrostat ($\beta = -3\pi/4$). Hence, the failure is again controlled by a shear crack with friction when the friction-locked zone ends. The critical crack plane is now tilted away from the σ_{11} axis since the lateral confining stress (σ_{33}) now becomes increasingly dominating for $-3\pi/4 \leqslant \beta \leqslant -\pi/2$. At $\beta = -\pi/2$, the material is under equal-biaxial compression in the σ_{22}–σ_{33} plane, which is equivalent to uniaxial compression along the σ_{33} direction for cracks with normal in the $\mathbf{e}_1$–$\mathbf{e}_3$ plane. Hence the failure angle with the $\mathbf{e}_1$ axis is just θ_c, as expected.

As β increases beyond $-\pi/2$, the stress state in the material becomes tension–compression ($\sigma_1 = \sigma_{11} > 0$, $\sigma_3 = \sigma_{33} < 0$). The failure type at first remains shear with friction until the tensile stress component reaches a critical value at which the type transitions to pure-shear. The failure type remains pure-shear until $\beta = -\pi/4$. Between the termination of pure-shear failure and the beginning of pure-opening, there exists a small region where the type of failure is mixed opening and shear. The failure angle during the transition from pure-shear failure to a pure-opening (mode-I) failure is not smooth. The critical angle θ^o given by Eq. (9) drops rapidly from 45° to 0° over a small range of load angles ($-45° \leqslant \beta \leqslant -\beta^o$; $\beta^o = 38.7°$ for $\nu = 0.2$). Then for $\beta \geqslant -\beta^o$, the failure angle remains at 0° (pure mode-I opening) until $\beta = \pi/4$ and then changes to 90° as σ_{33} becomes the dominant tensile stress. The behavior of the remaining portion of the curves ($\pi/4 \leqslant \beta \leqslant \pi$) is to be expected based on the assumption of an isotropic distribution of random cracks in the material.

The corresponding failure surfaces are shown in Fig. 5, where the axial and radial applied stresses are normalized with respect to the tensile strength of the material ($S_{\alpha\alpha} \equiv \sigma_{\alpha\alpha}/\sigma_o$; $\sigma_o \equiv S_{cr}(c)/\sqrt{1-\nu/2}$). It is shown that when the material is in a tension-dominated regime the current failure surface reduces to the maximum tension failure (Rankine) criterion, which is appropriate for a brittle material under tension. When compressive stress becomes dominant, the size of the failure surface increases with pressure and friction coefficient of the material, reproducing the Mohr–Coulomb failure surfaces. The failure surface transitions smoothly from the mode-I tensile failure to frictional shear failure. In this transition region, the material is under both tension and compression and fails by either a combination of mixed opening and shear, or pure-shear. These features seem to capture the failure of brittle materials under triaxial loading. The upper limit of $\mu = 2.0$ is chosen because the failure surfaces have reached their asymptotes there. In Fig. 5, we have terminated the failure surfaces in the compression region at $p = 5\sigma_o$ in order to show the features of both tensile and compressive failure. The actual failure surfaces are open-ended. In both Figs. 4 and 5, the Poisson's ratio is taken to be $\nu = 0.2$.

Fig. 6 is a diagram showing the various types of behavior that are possible in a brittle material under triaxial loading. There are five essentially different types. While the stress plane is divided into nine parts, symmetry reduces the essentially different kinds of behavior to five. Incipient failure is possible for sufficiently large stresses in any of the five segments except for the shear-locked zone where cracks are locked in compression. The value $\mu = 2.0$ is chosen here because this is our estimate of the typical friction coefficient in clean microcracks where there may be significant cohesion. Direct evidence for this behavior can be seen in the photographs and micrographs of damaged TNT presented by Howe et al. (1985). TNT is a good indicator of brittle behavior because the effects of frictional heating are easily observed. Pure-shear cracks (type **(c)**) can be observed in one portion of the target, while the effects of reaction caused by friction, a behavior of type **(d)**, are observed in a different section, as shown in Fig. 7. The sketch shows the actual cracks formed by impact of a flyer plate against the side of an artillery shell at 440 m/s. The filler explosive

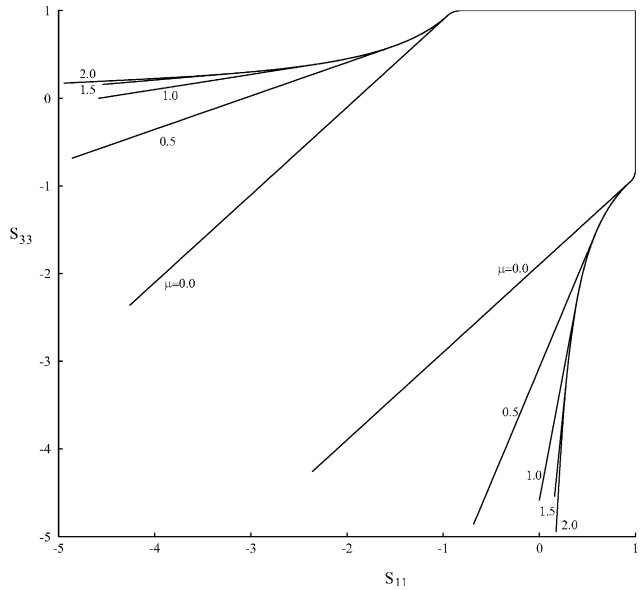

Fig. 5. Failure surfaces of a brittle material under triaxial loading for several values of friction coefficient, μ, from 0 to 2.0. Note that friction has no effect on the tensile failure, and that the compressive strength increases with pressure and friction coefficient. The surfaces nearly reach their asymptote at $\mu = 2.0$.

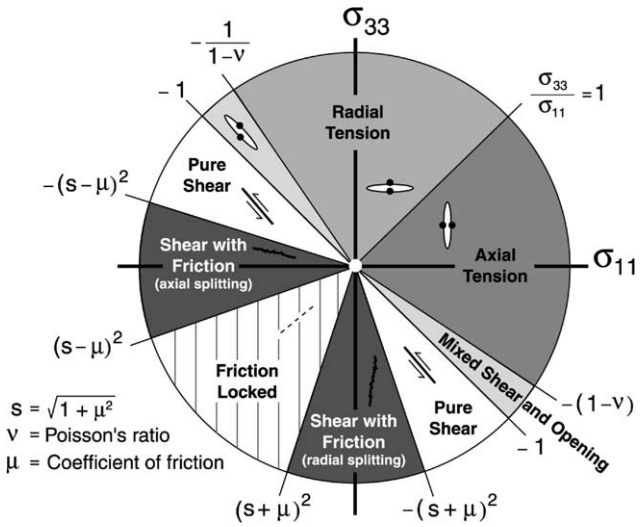

Fig. 6. A diagram showing the five types of response a brittle material can have under triaxial loading (σ_{11} and σ_{33} denote the axial and lateral stresses, respectively). For sufficiently high stress, axial and radial mode-I tensile failure can occur when tensile stress dominates (Type **(a)**); mixed opening and shear failure occurs over a small sector of the load angle (Type **(b)**); pure-shear (no normal traction) failure occurs for a range of stress states that can be significant if μ is large (Type **(c)**); "Splitting" occurs where the critical crack plane is nearly aligned with the greatest compression direction (Type **(d)**). A fifth type of response occurs when the stress state is sufficient close to hydrostatic compression so that the interfacial friction on a crack surface always exceeds the applied shear and as a result cracks are "friction-locked" (Type **(e)**).

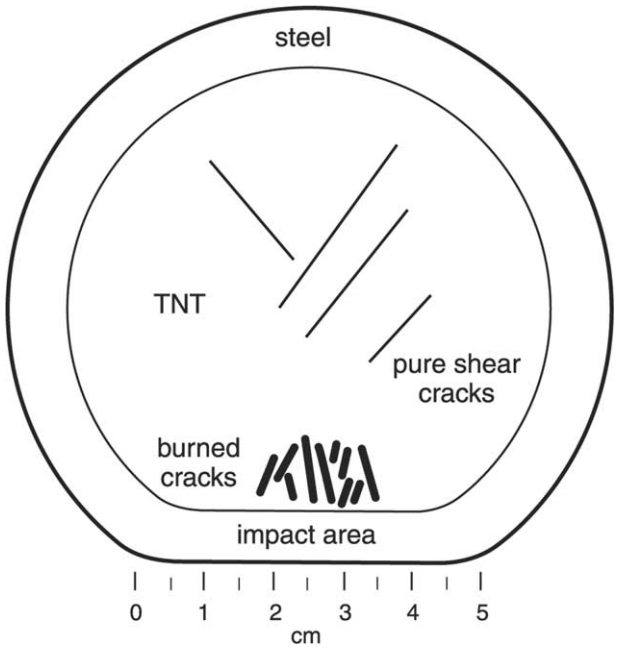

Fig. 7. A sketch showing the actual cracks formed by a flyer-plate impact at 440 m/s against the side of an artillery shell filled with TNT, as report by Howe et al. This illustrates the two types of shear cracks discussed on the text.

is TNT, a brittle material that is very sensitive to temperature. A micrograph of the long cracks at 45° to the impact direction shows no evidence of heating or reaction, though a shearing discontinuity is clearly evident. The short cracks show evidence of carbon formed by local heating. The sketch is a composite of two nearby sections of the shell that were carefully polished. A similar test at 680 m/s resulted in a violent explosion.

As an application of the instability criteria for penny-shaped cracks under combined normal and shear loadings, Keer (1966) generated the failure (fracture) surface for a brittle material under a biaxial state of stress which qualitatively agreed with experimental results for gray cast iron previously reported (reference cited in the paper). Since the effects of friction on crack instability were not accounted for, when the compressive stress is dominant the critical crack is always at 45° from the principal stress directions (the maximum shear plane) and the failure surface is parallel to the hydrostat. His results agree with the current work for $\mu = 0$, both in the failure orientations and the failure surface. However, the current work shows that for a frictional material there are several types of compressive behavior (pure-shear, shear with friction, friction locked), and the failure surface expands with increasing hydrostatic pressure and friction coefficient.

6. Summary and conclusions

We have presented an investigation of the effect of interfacial friction in penny-shaped cracks and, in particular, its influence on the most unstable crack orientation. The material is assumed to contain a random, isotropic distribution of penny-shaped cracks. Incipient failure is said to occur when the largest crack with critical orientation becomes unstable. When friction is accounted for it is found that, depending on the stress state, five types of brittle behavior are possible: **(a)** mode-I opening, **(b)** mixed opening and shear, **(c)** pure-shear without friction, and **(d)** shear with interfacial friction. A fifth type of behavior **(e)** occurs when the compressive traction on the crack is so large that friction inhibits crack growth. The first four types, namely, **(a)**, **(b)**, **(c)**, **(d)** result in material failure at sufficiently high stresses. We also give analytical expressions for the failure (critical crack) orientations in the principal stress basis.

When all the principal stresses are tensile, the critical crack normal aligns with the largest principal stress direction and the failure type is mode-I opening. When the material is completely under compression (all three principal stresses are compressive), the failure mode is always shearing with friction (but failure may not occur if the cracks are locked by friction). The most interesting case is when the principal stresses are of mixed signs. Here the failure type can be mode-I opening when the tensile stress dominates, or a combination of opening and shear when the magnitude of the compressive stress is less than but close to that of the tensile stress, or pure-shear when the compressive stress is larger than the tensile stress or, finally, shear with friction when the state of stress is close to uniaxial compression. For materials with high friction coefficient the pure-shear failure mode dominates over quite a sizable range of stress states.

We have also presented the failure surfaces in terms of the principal stresses. There are four surfaces and, depending on the stress state in the material, one of them will apply. The conditions for the applicability of the failure surfaces are also given explicitly in terms of the stress biaxialities. When the failure is controlled by a tensile or frictional crack, the failure surfaces are straight lines in the plane of maximum–minimum principal stresses. On the other hand, when the type of failure is pure-shear or mixed opening and shear, the surface is a segment of either a hyperbola or ellipse.

For materials with friction, there exists a range of compressive stress states over which shear cannot overcome friction. For those stress states, all cracks (hence the material) remain stable. We have presented the size of this "friction-locked zone", in terms of the load angle, as a function of the friction coefficient.

As an example, we have shown the failure orientation and failure surface of a brittle material under triaxial loading to illustrate the general framework presented in this paper. One perhaps surprising result is

that pure (frictionless) shear failure occupies a significant fraction of the stress states when the principal stresses are of mixed signs. This may explain one result of Howe et al. (1985) which shows damaged TNT (brittle explosive) recovered and polished following an impact test. Large cracks oriented at close to 45° to the impact direction are clearly shear cracks (no crack opening can be detected), but there is no evidence of melting or reaction (Fig. 7). Thus, there is clear evidence that friction is negligible, as would be expected when a pure-shear crack dominates. This, perhaps, provides an illustration of the pure-shear cracks expected from the theory, though the experiment involves a rather more complex stress history than the theory described here. On the other hand, cracks near the impact area show strong evidence of reactions because their orientation is nearly parallel to the impact direction, an unstable orientation according to our analysis for nearly uniaxial compression, and one that involves significant friction.

The interest in penny-shaped cracks stems in large part from their role in the construction of constitutive models for the behavior of brittle and quasi-brittle materials. For example, Dienes (1981) used such a model to explain the formation of an aspirin-shaped cavity in oil shale, a result of bedding cracks, as well as accounting for the impact sensitivity of a propellant (1996) and impact damage to alumina (Meyer et al., 1999). Addessio and Johnson (1990) modeled damage in ceramics (silicon carbides, boron carbides, titanium diborides) under impact condition. Their predictions compared favorably with shock compression and release experiments. Gambarotta and Lagomarsino (1993) succeeded in representing the brittle behavior of concrete during both loading and unloading. Bennett et al. (1998) modeled the dynamic response of an explosive by this means, and Guiton et al. (2003) accounted for the folding of sedimentary layers with such an approach. This list is not exhaustive. Additional work with such approaches is given in the references cited in these papers.

Acknowledgment

The authors are grateful to R.M. Brannon for her comments on the manuscript, and for her insights on the critical crack orientation which significantly simplified the analysis. Technical discussions with F.L. Addessio, P.J. Maudlin, M.W. Lewis, and H.L. Schreyer were also very helpful. This work was supported by the Joint Department of Energy (DOE) and Department of Defense (DoD) Munitions Technology Development Program, the DOE Accelerated Strategic Computing Initiative (ASCI), and the US Army Research Laboratory (Dr. W. Bruchey).

References

Addessio, F.L., Johnson, J.N., 1990. A constitutive model for the dynamic response of brittle materials. Journal of Applied Physics 67, 3275–3286.

Alpa, G., 1984. On a statistical approach to brittle rupture for multiaxial states of stress. Engineering Fracture Mechanics 19, 881–901.

Bennett, J.G., Haberman, K.S., Johnson, J.N., Asay, B.W., Henson, B.F., 1998. A constitutive model for the non-shock ignition and mechanical response of high explosives. Journal of the Mechanics and Physics of Solids 46, 2303–2322.

Dienes, J.K., 1981. On the effect of anisotropy in explosive fragmentation. In: Einstein, H.H. (Ed.), Rock Mechanics from Research to Application, Proceedings of the 22nd US Symposium on Rock Mechanics. MIT, Cambridge, MA.

Dienes, J.K., 1983. On the stability of shear cracks and the calculation of compressive strength. Journal of Geophysical Research 88, 1173–1179.

Dienes, J.K., 1984. Reply to comments on 'On the stability of shear cracks and the calculation of compressive strength' by J.R.Rice. Journal of Geophysical Research 89, 2508–2508.

Dienes, J.K., 1996. A unified theory of flow, hot spots, and fragmentation with an application to explosive sensitivity. In: Davison, L., Grady, D.E., Shahinpoor, M. (Eds.), High Pressure Shock Compression of Solids II. Springer Verlag, New York, pp. 366–398.

Dienes, J.K., Middleditch, J., Zuo, Q.H., Kershner, J.D., 2003. On the role of crack orientation in the brittle failure and the formation of hot spots. In: Furnish, M.D., Gupta, Y.M., Forbers, J.W. (Eds.), Shock Compression of Condensed Matter- 2003, AIP Conference Proceedings 706. Springer-Verlag, New York.

Fabrikant, V.I., 1989. Applications of Potential Theory in Mechanics. Kluwer Academic Publishers, Dordrecht.
Gambarotta, L., Lagomarsino, S., 1993. A microcrack damage model for brittle materials. International Journal of Solids and Structures 30, 177–198.
Guiton, M.L.E., Leroy, Y.M., Sassi, W., 2003. Activation of diffuse discontinuities and folding of sedimentary layers. Journal of Geophysical Research 108, 218301–218320.
Heaton, T.H., 1990. Evidence for and implications of self-healing pulses of slip in earthquake ruptures. Physics of the Earth and Planetary Interiors 64, 1–20.
Howe, P.M., Gibbons, G.G., Webber, P.E., 1985. An experimental investigation of the role of shearing initiation of detonation. In: Short, J.M., Deal, W.E. (Eds.), Proceedings of the 8th International Symposium on Detonation, Albuquerque, NM.
Kachanov, M.L., 1982a. A microcrack model of rock inelasticity, Part I: Frictional sliding on microcracks. Mechanics of Materials 1, 19–27.
Kachanov, M.L., 1982b. A microcrack model of rock inelasticity, Part II: Propagation of microcracks. Mechanics of Materials 1, 29–41.
Kalthoff, J.F., Winkler, S., 1987. Failure mode transition at high rates of shear loading. In: Chiem, C.Y., Kunze, H.D., Meyer, L.W. (Eds.), Impact Loading and Dynamic Behavior of Materials, vol. I. Springer-Verlag, Berlin, pp. 185–195.
Keer, L.M., 1964. Stress distribution at the edge of an equilibrium crack. Journal of Mechanics and Physics of Solids 12, 149–163.
Keer, L.M., 1966. A note on shear and combined loading for a penny-shaped crack. Journal of Mechanics and Physics of Solids 14, 1–6.
Lubliner, J., 1990. Plasticity Theory. Macmillan Publishing Company, New York.
Marsden, J.E., Hughes, T.J.R., 1983. Mathematical Foundation of Elasticity. Prentice-Hall, Englewood Cliffs, New Jersey.
McClintock, F.A., Walsh, J.B., 1962. Friction on Griffith cracks in rocks under pressure. In: Rosenberg, R.M. (Ed.), Proceedings of the Fourth US National Congress of Applied Mechanics. ASME, New York, pp. 1015–1021.
Meyer Jr., H.W., Abeln, T., Bingert, S., Bruchey, W.J., Brannon, R.M., Chhabildas, L.C., Dienes, J.K., Middleditch, J., 1999. Crack behavior of ballistically impacted ceramic. In: Furnish, M.D., Chhabildas, L.C., Hixson, R.S. (Eds.), Shock Compression of Condensed Matter, AIP Conference Proceedings 505. Springer-Verlag, New York.
Mura, T., 1991. Micromechanics of Defects in Solids, second, revised ed. Kluwer Academic Publishers, Dordrecht.
Rice, J.R., 1984. Comments on 'On the stability of shear cracks and the calculation of compressive strength' by J.K.Dienes. Journal of Geophysical Research 89, 2505–2507.
Rice, J.R., 2000. New perspectives on cracks and fault dynamics. In: Aref, H., Phillips, J.W. (Eds.), Mechanics for a New Millennium: Proceedings of the ICTAM 2000. Kluwer Academic Publishers, Dordrecht.
Rosakis, A.J., 2002. Intersonic shear cracks and fault ruptures. Advances in Physics 51, 1189–1257.
Sack, R.A., 1946. Extension of Griffith's theory of rupture to three dimensions. Proceedings of Physics Society 58, 729–736.
Schreyer, H.L., Wang, M.L., 1990. Elementary constitutive relations for Quasi-brittle materials based on continuum damage mechanics. In: Shah, S.P., Swartz, S.E., Wang, M.L. (Eds.), Micromechanics of Failure of Quasi-brittle Materials: Proceedings of International Conference of Micromechanics of Failure of Quasi-brittle Materials. Elsevier Applied Science Publication, New York.
Segedin, C.M., 1950. Note on a penny-shaped crack under shear. Proceedings of the Cambridge Philosophical Society 47, 396–400.
Smith, E., 1971. Note on the growth of a penny-shaped crack in a general uniform applied stress field. International Journal of Fracture Mechanics 7, 339–342.
Sneddon, I.N., 1946. The distribution of stress in the neighborhood of a crack in an elastic solid. Proceedings of the Royal Society of London 187A, 229–260.
Ulfyand, Ya.C., 1963. Integral Transforms in Problems of the Theory of Elasticity. Akad. Nauk. SSSR (in Russian).
Wei, K., De Bremaecker, J.-C., 1994. Fracture growth under compression. Journal of Geophysical Research 99, 13781–13790.